Antonio Miotello
Paolo M. Ossi
Editors

SPRINGER SERIES IN MATERIALS SCIENCE 130

Laser-Surface Interactions for New Materials Production

Tailoring Structure and Properties

Springer

Springer Series in
MATERIALS SCIENCE 130

Springer Series in

MATERIALS SCIENCE

The Springer Series in Materials Science covers the complete spectrum of materials physics, including fundamental principles, physical properties, materials theory and design. Recognizing the increasing importance of materials science in future device technologies, the book titles in this series reflect the state-of-the-art in understanding and controlling the structure and properties of all important classes of materials.

Antonio Miotello
Paolo M. Ossi
Editors

Laser-Surface Interactions for New Materials Production

Tailoring Structure and Properties

With 206 Figures

Springer

Editors

Professor Antonio Miotello
Università di Trento
Dipartimento di Fisica
Via Sommarive 14, 38050 Povo, Italy
E-mail: miotello@science.unitn.it

Professor Paolo M. Ossi
Politecnico di Milano
Dipartimento di Energia
Centre for NanoEngineered Materials
and Surfaces
via Ponzio 34-3, 20133 Milano, Italy
E-mail: paolo.ossi@polimi.it

Series Editors:

Professor Robert Hull
University of Virginia
Dept. of Materials Science and Engineering
Thornton Hall
Charlottesville, VA 22903-2442, USA

Professor Jürgen Parisi
Universität Oldenburg, Fachbereich Physik
Abt. Energie- und Halbleiterforschung
Carl-von-Ossietzky-Straße 9–11
26129 Oldenburg, Germany

Professor Chennupati Jagadish
Australian National University
Research School of Physics and Engineering
J4-22, Carver Building
Canberra ACT 0200, Australia

Dr. Zhiming Wang
University of Arkansas
Department of Physics
835 W. Dicknson St.
Fayetteville, AR 72701, USA

Professor R. M. Osgood, Jr.
Microelectronics Science Laboratory
Department of Electrical Engineering
Columbia University
Seeley W. Mudd Building
New York, NY 10027, USA

Professor Hans Warlimont
DSL Dresden Material-Innovation GmbH
Pirnaer Landstr. 176
01257 Dresden, Germany

Springer Series in Materials Science ISSN 0933-033X
ISBN 978-3-642-03306-3 e-ISBN 978-3-642-03307-0
DOI 10.1007/978-3-642-03307-0
Springer Heidelberg Dordrecht London New York

Library of Congress Control Number: 2009934001

Cover design: SPi Publisher Services

Printed on acid-free paper

Springer is part of Springer Science+Business Media (www.springer.com)

Preface

This book originates from lectures delivered at the First International School "*Laser-surface interactions for new materials production: tailoring structure and properties*" that was held in San Servolo Island, Venice (Italy) from 13 to 20 July, 2008 under the direction of A. Miotello and P.M. Ossi. The purpose of the School was to provide the students (mainly PhD) with a comprehensive overview of basic aspects and applications connected to the laser–matter interaction both to modify surface properties and to prepare new materials by pulsed laser deposition (PLD) at the nanometer scale. The field is relatively young and grew rapidly in the last 10 years because of the possibility of depositing virtually any material, including multi-component films, preserving the composition of the ablated target and generally avoiding post-deposition thermal treatments. In addition, the experimental setup for PLD is compatible with in situ diagnostics of both the plasma and the growing film.

The basic laser–surface interaction mechanisms, possibly in an ambient atmosphere, either chemically reactive or inert, are a challenge to scientists, while engineers are mostly interested in the characteristics of the deposited materials and the possibility of tailoring their properties through an appropriate tuning of the deposition parameters.

The School was motivated by the fact that while well established international conferences bring together many researchers every year and allow for extensive scientific exchange, the laser community was lacking a "teaching" event, specifically addressed to doctorate students and young post-docs to favour study of the deepening of the principles of laser–surface interactions, and to highlight the strong interplay between experimental and theoretical investigations of laser-induced phenomena.

Lecturers, coming from both the academy and leading research centers are actively contributing to research topics addressed during the School; we are grateful to them for the attention they gave to arranging presentations having a truly didactic, though high level, character. In addition, they maintained constructive interactions with the students throughout the School duration and prepared texts of their lectures in time for this book.

The result is an updated overview concerning laser induced phenomena on both the nanosecond and ultra-short timescale, together with pertinent diagnostics; material classes span from polymers to ceramics and metals, including piezoelectrics, ferroelectrics, biomaterials, glasses, and functional coatings. Laser direct writing, lasers in cultural heritage and MAPLE are considered and computer modelling is focussed both on atomic-level simulations and on continuum models.

Highlights of the present book reflect the guidelines of the School: they include topics that gained relevance in the scientific community in recent years, such as ultra-short laser pulses to explore electronic excitation in solids and its relaxation with phonons in highly non equilibrium conditions, surface melting, vapourisation, superheating, homogeneous and possibly heterogeneous nucleation, the synthesis of nanometer scale clusters and their assembling to prepare nanocrystalline films.

The School was hosted by Venice International University (VIU) at its quarters at S. Servolo Island, a site in the centre of the city, with a fascinating, long standing history. The site was recently restored to be used for cultural events providing a highly agreeable working ambient. The directors are grateful to the staff of VIU for the excellent organisation and hospitality.

To facilitate the exchange of scientific experiences and to benefit from the inspiring atmosphere enjoyed at S. Servolo, the number of students was limited. A total of 42 participants, most of them Ph.D. students, or young post-doc researchers, were selected from 22 Countries; although most of them originated from EU, students from Russia, USA, India, Pakistan, and Japan attended the School.

All students contributed to the activities of the School during the discussions throughout the lectures, and by bringing posters of their research activity. The posters were exhibited in the lecture hall for the entire duration of the School and were extensively discussed during three poster sessions. Students' participation in the School was facilitated by the support of the Politecnico di Milano, the University of Trento, and several industrial sponsors.

The positive evaluation of the students convinced the organising committee to plan the Second International School on "*Laser-surface interactions for new materials production*," to be held in S. Servolo Island from 11 to 18 July 2010, under the direction of C. Boulmer-Leborgne, M. Dinescu, T. Dickinson and P.M. Ossi.

Trento, Milano — *A. Miotello*
October 2009 — *P.M. Ossi*

Contents

List of Contributors

Ratiba Benzerga
Université d'Orléans-CNRS, GREMI, Polytech, BP 6744, Orléans cedex2, France

Adriana Bigi
Department of Chemistry "G. Ciamician," University of Bologna, via Selmi, 2, Bologna 40126, Italy

Chantal Boulmer-Leborgne
Université d'Orléans-CNRS, GREMI, Polytech, BP 6744, Orléans cedex2, France

Nadezhda M. Bulgakova
Institute of Thermophysics SB RAS, prosp. Lavrentyev, 1, 630090 Novosibirsk, Russia, nbul@itp.nsc.ru

Anna Paola Caricato
Università del Salento, Dipartimento di Fisica, 73100 Lecce, Italy

Douglas B. Chrisey
Material Science and Engineering, Rensselaer Polytechnic Institute, 110 Eighth Street, Troy, NY 12180, USA

David T. Corr
Departments of Biomedical Engineering, Rensselaer Polytechnic Institute, 110 Eighth Street, Troy, NY 12180, USA

Maria Dinescu
National Institute for Lasers, Plasma and Radiation Physics, Bucharest, Romania, dinescum@ifin.nipne.ro

William H. Duff
Department of Materials Science & Engineering, University of Virginia, 395 McCormick Road, Charlottesville, VA 22904-4745, USA

Gyula Eres
Materials Sciences and Technology Divisions, Oak Ridge National Laboratory, Oak Ridge, TN 37831, USA

David B. Geohegan
Center for Nanophase Materials Sciences, Oak Ridge National Laboratory, Oak Ridge, TN 37831, USA
and
Materials Sciences and Technology Divisions, Oak Ridge National

Laboratory, Oak Ridge, TN 37831, USA
geohegandb@ornl.gov

Stephen J. Guy
Department of Materials Science & Engineering, University of Virginia, 395 McCormick Road, Charlottesville, VA 22904–4745, USA

Richard F. Haglund
Department of Physics and Astronomy, Vanderbilt University, 2201 West End Avenue, Nashville, TN 37240, USA

Ingolf V. Hertel
Department of Physics, Free University of Berlin, Arnimallee 14, 14195 Berlin, Germany
and
Max-Born-Institut für Nichtlineare Optik und Kurzzeitspektroskopie, Max-Born Str. 2a, 12489 Berlin, Germany

Daniel Höche
Universität Göttingen, Zweites Physikalisches Institut, Friedrich-Hund-Platz 1, 37077 Göttingen, Germany

Hui Hu
Materials Sciences and Technology Divisions, Oak Ridge National Laboratory, Oak Ridge, TN 37831, USA

Ilia Ivanov
Center for Nanophase Materials Sciences, Oak Ridge National Laboratory, Oak Ridge, TN 37831, USA
and
Materials Sciences and Technology Divisions, Oak Ridge National Laboratory, Oak Ridge, TN 37831, USA

Dmitriy S. Ivanov
Department of Materials Science & Engineering, University of Virginia, 395 McCormick Road, Charlottesville, VA 22904-4745, USA

Jeremy Jackson
Center for Nanophase Materials Sciences, Oak Ridge National Laboratory, Oak Ridge, TN 37831, USA
and
Materials Sciences and Technology Divisions, Oak Ridge National Laboratory, Oak Ridge, TN 37831, USA

Stephen L. Johnson
Department of Physics, University of Kentucky, Lexington, KY 40506, USA

Wolfgang Kautek
University of Vienna, Department of Physical Chemistry, Waehringer Strasse 42, A-1090 Vienna, Austria,
wolfgang.kautek@univie.ac.at

Elodie Leveugle
Department of Materials Science & Engineering, University of Virginia, 395 McCormick Road, Charlottesville, VA 22904–4745, USA

Zhibin Lin
Department of Materials Science & Engineering, University of Virginia, 395 McCormick Road, Charlottesville, VA 22904-4745, USA

Thomas Lippert
General Energy Department, Paul Scherrer Institut, CH-5232 Villigen PSI, Switzerland

Zuqin Liu
Center for Nanophase Materials Sciences, Oak Ridge National Laboratory, Oak Ridge, TN 37831, USA

Armando Luches
Università del Salento, Dipartimento di Fisica, 73100 Lecce, Italy

Isaac Mayer
Institute of Chemistry, The Hebrew University of Jerusalem, 91904 Jerusalem, Israel

Ion N. Mihailescu
National Institute for Lasers, Plasma and Radiation Physics, Box MG-54, RO-77125 Bucharest, Magurele, Romania, ion.mihailescu@inflpr.ro

Karren More
Materials Sciences and Technology Divisions, Oak Ridge National Laboratory, Oak Ridge, TN 37831, USA

Paolo M. Ossi
Dipartimento di Energia, Politecnico di Milano, via Ponzio, 34–3, 20133 Milano, Italy, paolo.ossi@polimi.it

Michael R. Papantonakis
Naval Research Laboratory, 4555 Overlook Avenue, SW, Washington, DC 20375, USA

Jacques Perrière
INSP, Université Pierre et Marie Curie-Paris 6, CNRS UMR 7588, Campus Boucicaut, 140 rue de Lourmel, 75015 Paris, France

Alex A. Puretzky
Center for Nanophase Materials Sciences, Oak Ridge National Laboratory, Oak Ridge, TN 37831, USA
and
Materials Sciences and Technology Divisions, Oak Ridge National Laboratory, Oak Ridge, TN 37831, USA

Juergen Reif
Brandenburgische Technische Universität, BTU Cottbus *and* Cottbus JointLab, Universitätsstrasse 1, 03046 Cottbus, Germany, reif@tu-cottbus.de

Carmen Ristoscu
National Institute for Lasers, Plasma and Radiation Physics, Box MG-54, RO-77125 Bucharest, Magurele, Romania

Arkadi Rosenfeld
Max-Born-Institut für Nichtlineare Optik und Kurzzeitspektroskopie, Max-Born Str. 2a, 12489 Berlin, Germany

Chris Rouleau
Center for Nanophase Materials Sciences, Oak Ridge National Laboratory, Oak Ridge, TN 37831, USA
and
Materials Sciences and Technology Divisions, Oak Ridge National Laboratory, Oak Ridge, TN 37831, USA

Peter Schaaf
TU Ilmenau, Institut für Werkstofftechnik, Werkstoffe der Elektrotechnik, Postfach 100565, 98684 Ilmenau, Germany, peter.schaaf@tu-ilmenau.de

Nathan R. Schiele
Departments of Biomedical Engineering, Rensselaer Polytechnic Institute, 110 Eighth Street, Troy, NY 12180, USA

Carlos Sevilla
Department of Materials Science & Engineering, University of Virginia, 395 McCormick Road, Charlottesville, VA 22904-4745, USA

Razvan Stoian
Laboratoire Hubert Curien (UMR 5516 CNRS), Université Jean Monnet, 18 rue Benoit Lauras, 42000 Saint Etienne, France

David Styers-Barnett
Center for Nanophase Materials Sciences, Oak Ridge National Laboratory, Oak Ridge, TN 37831, USA

Koji Sugioka
RIKEN – The Institute of Physical and Chemical Research
2-1 Hirosawa,Wako, Saitama 351-01, Japan,
ksugioka@postman.riken.jp

Derek Thomas
Department of Materials Science & Engineering, University of Virginia, 395 McCormick Road, Charlottesville, VA 22904-4745, USA

Kai Xiao
Center for Nanophase Materials Sciences, Oak Ridge National Laboratory 1 Bethel Valley Road, Oak Ridge, TN 37831-6030, USA.

Bin Zhao
Center for Nanophase Materials Sciences, Oak Ridge National Laboratory, Oak Ridge, TN 37831, USA

Leonid V. Zhigilei
Department of Materials Science & Engineering, University of Virginia, 395 McCormick Road, Charlottesville, VA 22904-4745, USA
lz2n@virginia.edu

1

Laser Interactions in Nanomaterials Synthesis

David B. Geohegan, Alex A. Puretzky, Chris Rouleau, Jeremy Jackson, Gyula Eres, Zuqin Liu, David Styers-Barnett, Hui Hu, Bin Zhao, Ilia Ivanov, Kai Xiao, and Karren More

Summary. Laser interactions with materials have unique advantages for exploring the rapid synthesis, processing, and in situ characterization of high-quality and novel nanoparticles, nanotubes, and nanowires. For example, laser vaporization of solids into background gases provides a wide range of processing conditions for the formation of nanomaterials by both catalyst-free and catalyst-assisted growth processes. Laser interactions with the growing nanomaterials provide remote in situ characterization of their size, structure, and composition with unprecedented temporal resolution. In this article, laser interactions involved in the synthesis of primarily carbon nanostructures are reviewed, including the catalyst-free synthesis of single-walled carbon nanohorns and quantum dots, to the catalyst-assisted growth of single- and multi-walled carbon nanotubes.

1.1 Introduction

Laser vaporization of solid targets has long been a tool for the synthesis and discovery of clusters by mass spectrometry [1], resulting in the discovery of C_{60} and higher fullerenes in 1985 [2]. Two years later, yttrium–barium–copper oxide, high-temperature superconductors were discovered, and commercial excimer lasers were found to congruently vaporize multicomponent targets to grow thin films of these materials [3], fueling a resurgence of interest in pulsed laser deposition (PLD) for materials discovery, and a need to more fully understand the laser vaporization process [4]. In 1996, while trying to develop a catalyst-assisted process for the mass production of fullerenes, laser vaporization of a multicomponent (carbon and metal catalyst) target into flowing argon gas at high temperatures ($1,100°C$) resulted in the synthesis of single-wall carbon nanotubes (SWNTs), a major breakthrough in their production [5]. In 1998, this laser vaporization technique was generalized for the VLS-synthesis of semiconducting nanowires [6,7], further emphasizing the role of lasers in the exploration of new nanomaterials. These discoveries were highly instrumental in the development of an understanding of the synthesis of nanomaterials. In this article, we will outline some of the key processes governing the synthesis of nanomaterials by laser-driven interactions, with a special emphasis on carbon materials.

1.2 Laser Ablation and Plume Thermalization at Low Pressures

The virtues of laser ablation for the PLD of thin films primarily involve the rapid, stoichiometric removal and atomization of a solid, and the formation of an energetic beam of neutrals, ions, small molecules, and clusters [4]. The laser interaction with the solid usually forms a dense laser plasma ($T_e \sim 1$–$10\,\mathrm{eV}$), which expands and cools during a period of collisions near the target surface in which fast ions, slower neutrals, and even slower molecules and clusters emerge with a shifted, center-of-mass Maxwell-Boltzmann velocity distribution. Despite disparate masses, atoms in a multicomponent target often travel at nearly the same velocity when they emerge from this collisional "Knudsen layer," with atoms near the peak of the distribution typically moving at velocities $v \sim 1\,\mathrm{cm\,\mu s^{-1}}$, corresponding to significant kinetic energies ($\sim$10–100 eV).

However, immediately following laser vaporization, oxidation and other chemical reactions can occur in the early portions of the plume expansion to form new molecules and clusters. In addition, since nanosecond or longer pulses are typically utilized, the laser may interact with the ejecta as they expand, resulting in photodissociation of clusters, photoionization of neutrals, and other processes that result in regional heating and secondary plume dynamics. An example of this is shown in Fig. 1.1, where pyrolytic graphite is ablated by ArF (193 nm) and KrF (248 nm) lasers in vacuum [8, 9].

Stepwise increases in laser intensity results in the appearance of distinct regions of plasma luminescence: first, from excited primary ejecta C_3 and C_2; second, from atomic carbon resulting from photodissociation of C_2; and

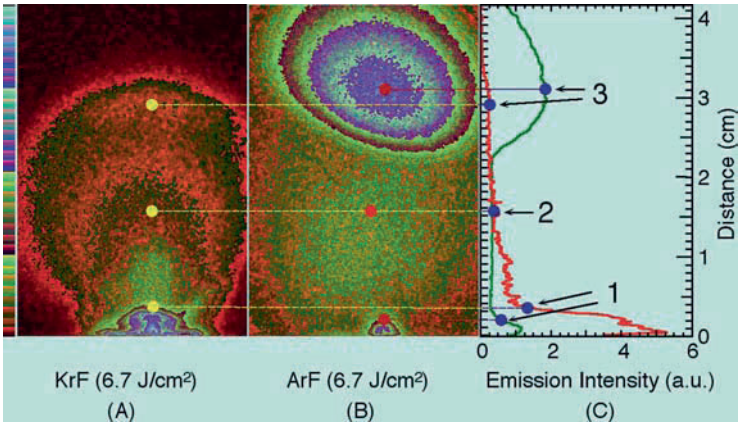

Fig. 1.1. ICCD images of visible plume emission from KrF-laser (248 nm) and ArF-laser (193 nm) ablated pyrolytic graphite in vacuum, taken $\Delta t = 1.0$ μs following ablation. Three regions of plume emission are observed, corresponding to (1) C_2 and C_3, (2) C, and (3) C^+. (Reproduced with permission from [8])

third, a fast ball of C^+ ions resulting from two-photon, resonant ionization of atomic C (Reproduced with permission from [10]). The interplume dynamics, which result in the selective acceleration of the C and C^+, are observed to retard the expansion of the slower C_2 and C_3, inducing additional collisions and more clustering, and redeposition of these materials on the target surface. Thus, the choice of laser wavelength can influence the composition, kinetic energies, and trajectories of the initial ejecta from the target.

The addition of a low-pressure background gas results in collisions which slow the plume and confine it, often with the inadvertent formation of nanoparticles. Fig. 1.2a shows a sequence of images of the plume resulting from

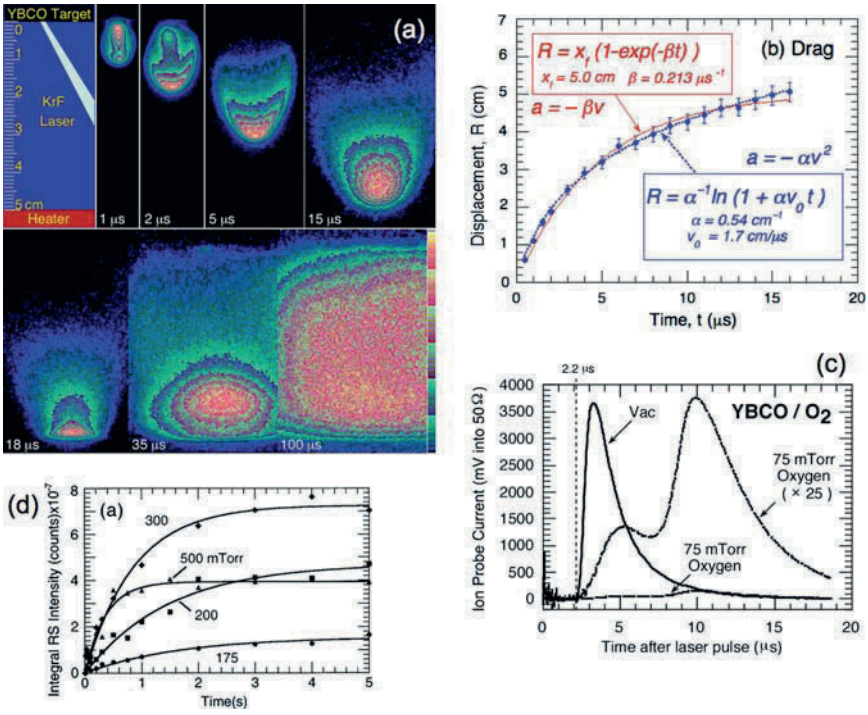

Fig. 1.2. (**a**) Side-on, false-color ICCD images of visible plume emission from YBCO ablated in 200 mTorr oxygen at the indicated times. Although initially moving at leading edge velocities of 1 cm/μs, the plume arrives at a heater surface 5 cm away at $\Delta t = 15$ μs. The plume does not entirely deposit, but rebounds to fill the region between the heater and target [10]. (**b**) The propagation of the leading edge of the plume is adequately represented by phenomenologic drag models. (**c**) However, ion probe flux measurements reveal a "splitting" of the plume at certain distances and pressures which has only been adequately explained by an elastic collision model [10]. (**d**) Integrated intensities from Rayleigh scattering images of the region between the target and heater show the time dependences of nanoparticle growth at pressures typically used for PLD. [Adapted from 8, 9, 11]

YBCO ablation into 200-mTorr oxygen. Collisions of the plume atoms and ions with the background gas lead to bright, recombination-fed fluorescence. Although this bright "shock front" progression can be adequately represented by shock and drag models [4], two components of the plume coexist for a given range of distances for a particular background pressure, as revealed by ion flux measurements as in Fig. 1.2c. This "plume splitting" has been analyzed and modeled to result from elastic collisions, which scatter and delay the plume atoms [11,12]. The two peaks roughly correspond to a fast distribution of material, exponentially decaying with distance or pressure, of original plume material which has undergone few if any collisions – and a slowed peak which has undergone one or more collisions. After all the plume atoms have undergone several collisions, they form a slowed, propagating front of material which collides with a cold heater surface in Fig. 1.2a (*lower panel*). A large fraction of the material does not stick to the heater surface, and slowly it rebounds. During the next several seconds (Fig. 1.2d), laser-induced fluorescence imaging and Rayleigh-scattering (RS) imaging (not shown) reveal that oxide clusters and nanoparticles slowly grow from this residual material for pressures above 175 mTorr under typical experimental conditions used for PLD film growth [13]. Interestingly, the imaging of Rayleigh-scattered light from a time-delayed, 308-nm laser sheet revealed that this process is highly quenched by the application of a small-temperature gradient, which flushes the nanoparticles from the region as they begin to form [13].

1.3 Synthesis of Nanoparticles by Laser Vaporization

Novel-new nanomaterials can be formed by laser vaporization into high-pressure background gases [14, 15]. The process can be modeled by an isentropic expansion of a gas [16]; however, the actual dynamics are of interest in order to control the synthesis process. Figure 1.3 shows the plume expansion following laser vaporization of Si into 10 Torr He, for the formation of brightly photoluminescent SiO_x nanoparticles. For the first 400 μs, the plasma emission can be directly imaged; however, for longer times, a second, time-delayed (308 nm) laser is used to induce luminescence from the plume. In this case, for times >200 μs, the photoluminescence from small clusters and nanoparticles formed in the plume is used to reveal their position and dynamics [17].

As the images show, a very bright region of photoluminescent clusters is formed behind the leading edge of the plume. These clusters were too small, however, to scatter light sufficiently for RS imaging. The nanoparticles grow and consolidate on the leading edge of the plume within 1 ms, and the swirling, forward-moving, vortex dynamics segregate the particles within a "smoke ring". The smoke ring continues forward to encounter a stationary Si wafer at room temperature however the nanoparticles do not stick, but remain there for several seconds until they agglomerate, at which point photoluminescence is quenched.

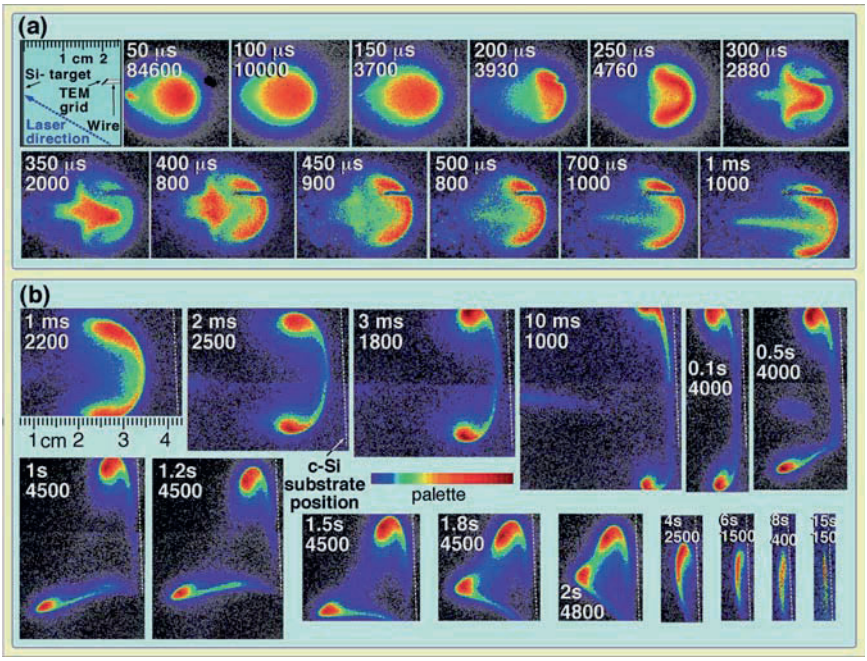

Fig. 1.3. (**a**) ICCD images of plasma luminescence ($\Delta < 400$ μs) plus photoluminescence ($\Delta t > 200$ μs) from nanoparticles produced by silicon ablation into 10 Torr He (3 μs exposures) at the indicated times and peak image intensities. (**b**) PL images utilizing a sheet of 308-nm laser light at later times show a slice through a swirling smoke ring of nanoparticles, and the nanoparticles encountering a room-temperature silicon wafer (at the *dashed line* position). The movement of the lower portion of the nanoparticle cloud is due to a very weak gas flow in the chamber caused by the gas introduction [17]

These dynamics are quite unlike the expansion of ablated Si into background Argon (not shown). The high-relative atomic mass of Ar vs. Si (40 vs. 28) induces a significant slowing of the plume compared to the Si/He case (28 vs. 4). Just 1 Torr of Ar produces a stopped and stationary cloud of nanoparticles (as revealed by RS imaging) without the turbulent motion needed to draw in oxygen required for oxidation into SiOx. Thus, without an intentional flow of Ar to introduce trace impurities of oxygen, no PL is observed. The choice of background gas can, therefore, significantly affect the propagation of the plume and its chemistry.

1.4 Self-Assembly of Carbon Fullerenes and Nanohorns

Carbon fullerenes were discovered in 1985 by the laser ablation of carbon into the high-pressure background gas within a specially constructed, windowed-pulsed nozzle source [2]. Soon after, laser vaporization of graphite targets

within a hot tube furnace was used to scale the production of fullerenes to laboratory scale, which was followed by electric arc vaporization for mass production [18]. Theoretical modeling of the synthesis process has shown that high temperatures of ∼3,000 K are required to induce the curvature that is necessary for the formation of fullerenes and other curved carbon nanostructures. Synthesis temperatures of ∼1,000–2,000 K produce flat carbon chain structures and sheets. Yet, fullerenes and other larger nanostructures can be produced by laser vaporization into room-temperature background ambients.

To understand the timescales, temperatures, and dynamics that are involved in fullerene production, time-resolved imaging and spectroscopy of the laser vaporization of carbon into room temperature 300 Torr Ar gas were performed (Fig. 1.4). The images show a confined plume with a series of highly reproducible shock waves which correspond to regions of plume expansion and cooling. The initial expansion of high-density C atoms and ions is rapidly stopped (300 ns) and a backward-propagating rarefaction wave is formed. This

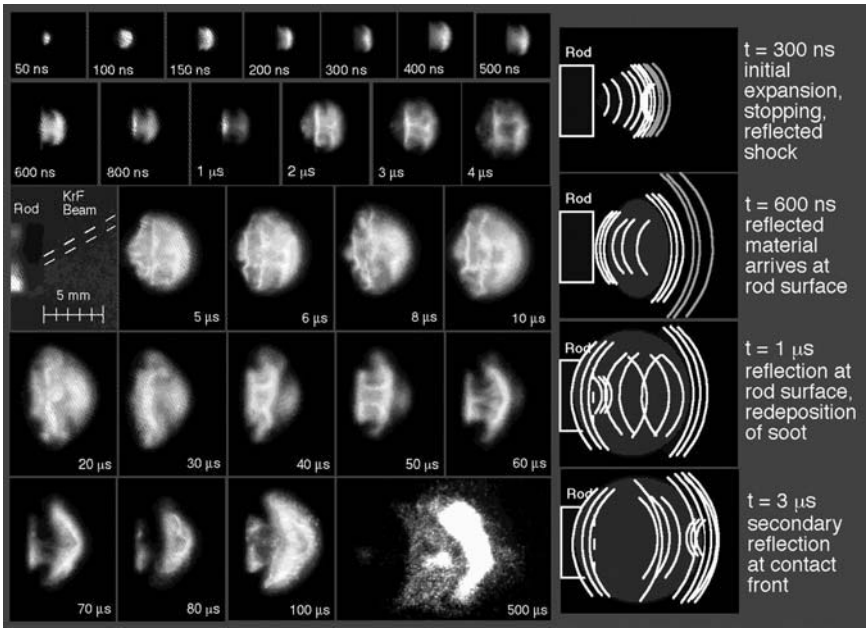

Fig. 1.4. (**a**) ICCD images of the interplume shock dynamics resulting from laser vaporization of C into 300 Torr Ar at room temperature for the formation of fullerenes. The small quantity of ablated C is quickly (300 ns) stopped, and a reflected shock drives material back toward the target. Reflected shocks continue, the plume expanding in oscillations, until a final push occurs in a mushroom cloud expansion where glowing clusters can be observed (at 500 μs) [19]

wave arrives at and reflects from the target surface from $\Delta t = 0.6$–$1.0\,\mu s$, and the plume is observed to oscillate and expand in stages as the material oscillates between the contact front with the ambient gas and the target surface. During the process, the material deposits on the target; however, no fullerenes are found there. The growth of the fullerenes occurs over extended times, during the final expansion of the plume for $t > 30\,\mu s$ after ablation. During this time, the plume cools from ~3,000 K to ~1,000 K, as recorded by blackbody emission from hot clusters and particulates in the plume (as in 500 μs image in Fig. 1.4). Experimentally, the choice of background gas and pressure is found to govern the extent of plume confinement and the rate of cooling within the volume, which serves as the substrateless microreactor where nanoparticle growth takes place [19].

In 1999, much larger carbon nanostructures – single-wall carbon nanohorns (SWNHs) – were reported by a similar laser vaporization process, however at much higher laser power [20]. SWNHs are tubular shaped, single-wall carbon nanostructures (like SWNTs); however, they are produced *without catalysts.* The synthesis process was not understood; however, similar multi-walled tubular structures were formed in 1994 when "fullerene soot" from an arc reactor was annealed at high temperatures *ex situ*, indicating that in addition to completed fullerenes, incomplete carbon structures had been formed and were capable of further assembly [21]. The ablation of C targets into room temperature, and atmospheric pressure background gases of He and Ar were found to form different flower-shaped aggregates of the nanohorns, including "dahlia-like" and "bud-like" nanohorns [22].

Recently, we applied tunable laser pulses to investigate the timescales and dynamics of SWNH growth [23, 24]. By varying both the energy and the pulse width of a high-power (600-W average power) laser, different ablation regimes could be explored. To explore the carbon nanostructures formed under long, *continuous* heating, and ablation, the laser pulse width was adjusted to multi-millisecond lengths, and high energies (up to 100 J per pulse) were used. To explore nanostructures formed under shorter plume lifetimes, sub-millisecond pulses and low (~1–5 J per pulse) laser energies were used. The temperature of the target surface was recorded by fast, optical pyrometry during laser irradiation, and compared to a three-dimensional, finite-element model simulation that included heating with a laser beam, heat losses due to heat conduction, target evaporation, blackbody radiation, and cooling by the surrounding buffer gas. The results are summarized in Fig. 1.5. Cumulative laser vaporization with 1 J pulses was found to require ~10 laser pulses before the surface temperature was sufficient (3,750°C) to vaporize C; however, once achieved a steady ablation rate of $\sim 6\,g\,h^{-1}$ was found to be very comparable to that using high-energy individual pulses for the same ~500 W average laser power. On the other hand, individual high-energy (~100 J) pulses of 10–20 ms duration were sufficient to rapidly heat the target to 4,200°C, and maintain vaporization in a *continuous* ablation mode. High-speed videography was used to record the heating and cooling times of the plume for

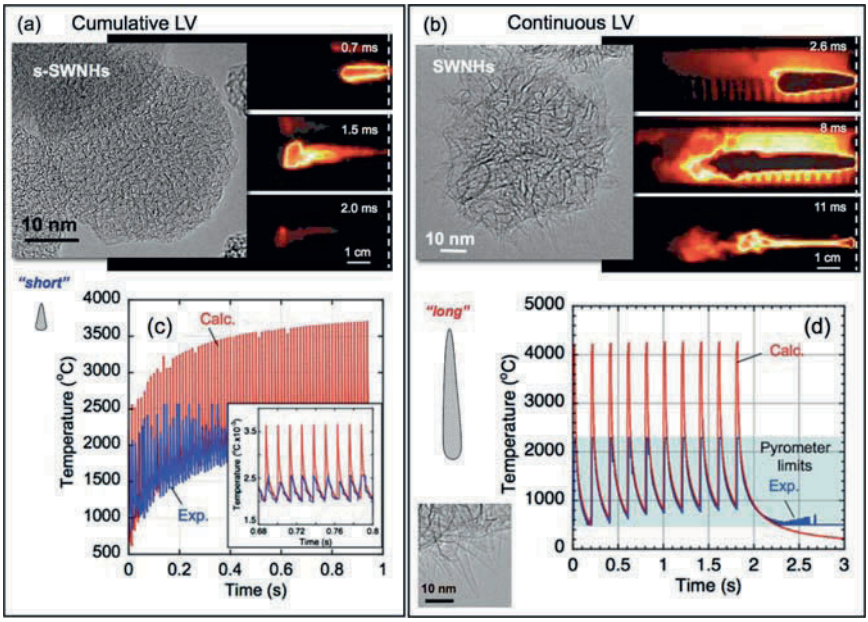

Fig. 1.5. (**a**, **b**) Selected frames from high-speed (50,000 fps) video images recorded in situ from within a 1,150 ° C tube furnace during high-power laser vaporization of C targets using (**a**) *cumulative* ablation (from 1 ms, 9 J laser pulses, at 50 Hz) and (**b**) *continuous* ablation (10 ms, 90 J laser pulses, 5 Hz). Variation of the laser pulse widths and energies can be used to adjust the times and temperatures available for single-wall carbon nanotube and nanohorn growth. HRTEM images show representative materials collected outside the furnace following the synthesis events illustrated by the time-resolved image sequences. (**c**) and (**d**) illustrate in situ pyrometry of the target surface and calculated temperature profiles from a 3D heat transfer simulation of the target heating. Parameters are (**c**) (20 ms pulses, 100 J/pulse, at 5 Hz) and (**d**) short pulses (0.5 ms pulses, 5 J/pulse at 80 Hz). The highlighted horizontal band in (**d**) shows the pyrometer limits. After [23, 24]

comparison with the quite different, nanohorn structures obtained in the different modes. As indicated in Fig. 1.5a, b, high-resolution TEM images show a variation in both the size of the individual nanohorn subunit, as well as the size of the aggregate structures which are formed. The length of nanohorn was found to correlate well with the time spent within the high-temperature growth zone, with the length increasing at a rate of $\sim$1 nm ms^{-1} of the available growth time. This rate is highly comparable to the $\sim$1–5 cm µs^{-1} rates found for catalyst-assisted SWNT growth, indicating that C can self-assemble into nanostructures at rates comparable to those using catalyst assistance [24].

1.5 Catalyst-Assisted Synthesis of SWNTs

Laser vaporization of carbon targets containing ∼1–2 at % metal catalyst powders (e.g. Ni and Co), is a very effective technique to produce exclusively SWNTs at ∼1,200°C in flowing Ar [25]. As summarized in Fig. 1.6, in situ

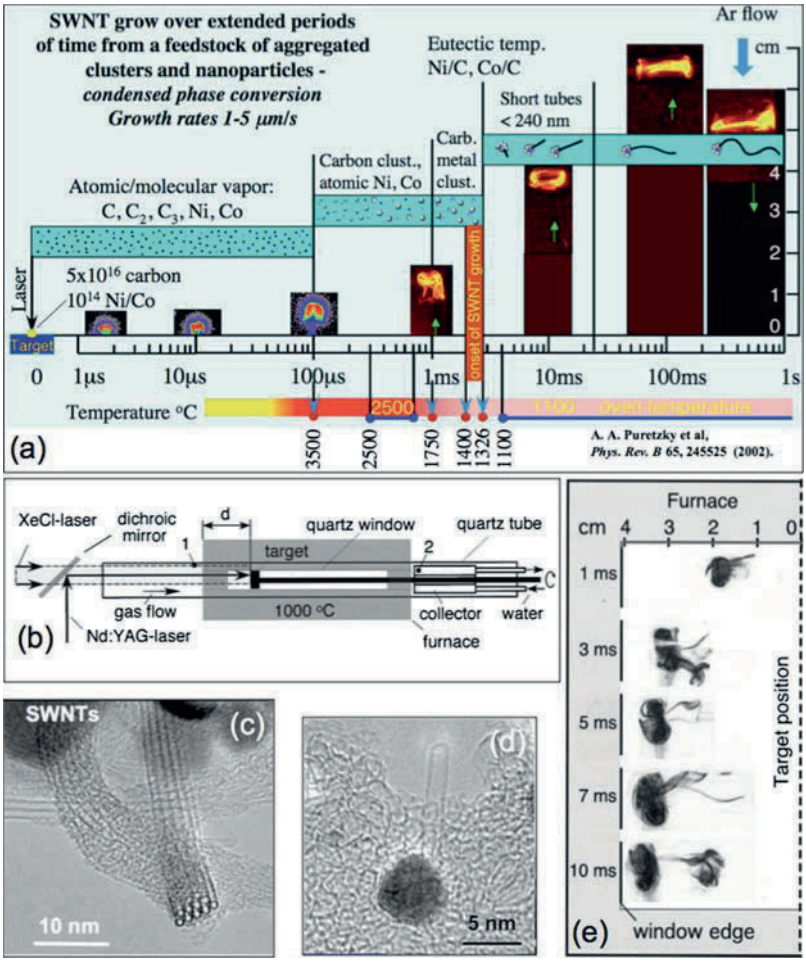

Fig. 1.6. (**a**) Summary of time-resolved imaging, spectroscopy, and temperature measurements of SWNT synthesis by laser vaporization. SWNT growth occurs at extended times from condensed carbon confined within a vortex ring at rates of 1–5 μ/s. **(b)** Schematic of the windowed laser oven used in the time-restricted growth experiments incorporating a second, time-delayed XeCl laser. (**c**) SWNT bundle typical of extended growth times (**d**) Short SWNT "seed" emanating from a 5 nm NiCo nanoparticle resulting from time-restricted growth (**e**) Rayleigh scattering images of the plume formed within the windowed portion of the furnace, just prior to exiting the furnace for rapid quenching of the growth. After [27]

imaging and spectroscopy studies of the ns-laser vaporization process revealed that (a) both carbon and metal are principally in the form of atoms and molecules (C, C_2, C_3, Ni, Co) during the first 100 μs, when the plume of ejecta are within ∼1 cm of the target, (b) that carbon forms clusters within 1 ms after laser vaporization, as the hot plasma cools, and that (c) Ni and Co form clusters later in time (1 ms $< t <$ 2 ms) after laser ablation [10, 26]. Through stop-growth experiments, where the plume was ejected from the hot oven after different growth periods (as revealed by imaging the plume via Rayleigh scattering shown in Fig. 1.5e), it was learned that only short SWNT "seeds" or nuclei had formed after 15–20 ms of growth time. By adjustment of this time, a growth rate in the range of 1–5 $\mu m\,s^{-1}$ could be inferred for SWNT growth by laser vaporization [27].

It was concluded that one of the main conditions to achieve a high yield of SWNTs was confinement of the ejected material inside the propagating laser plume, and that the main mechanism of this confinement was formation of a vortex ring. We recently showed that the confined volume could be significantly reduced if *cumulative ablation* using a sequence of pulses with a relatively low peak power (described above) was used to ablate the target, instead of individual ns-laser pulses with high-peak powers. The detailed study of this laser ablation regime revealed that preheating of the target with approximately 10 laser pulses is required to achieve stationary ablation. Weight analysis of the target and HRTEM of the products revealed that, averaged over many pulses the same ablation rates were achieved for the same input total energy between single- and multi-shot ablation, but higher conversion efficiencies of carbon to SWNTs were obtained when the ejected material was confined in a smaller volume [23]. Therefore, this cumulative regime of laser ablation is very useful for synthesis of SWNTs and other nanomaterials when long-term confinement of the ablated material is required.

1.6 Laser Diagnostics and Controlled Chemical Vapor Deposition of Carbon Nanotubes

As described in Fig. 1.7, laser-based diagnostics have also been applied recently to understand and control the growth of carbon nanotubes by chemical vapor deposition (CVD), providing some of the first direct kinetics measurements and growth rates measured in situ [28, 29].

Using the results from in situ growth rate measurements in which temperature, gas flow, and hydrocarbon concentration were varied, a kinetics model was developed to fit the measured growth rates and terminal lengths of vertically-aligned carbon nanotube arrays (VANTAs). Activation energies for the different processes were determined, and the optimal growth conditions to produce long nanotube arrays were predicted [29]. By measuring the number of walls for the nanotubes grown under different conditions, it was possible

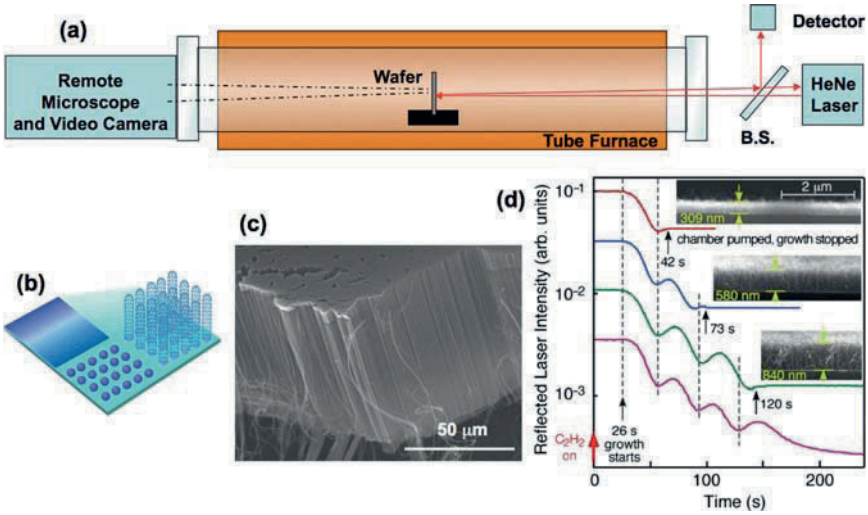

Fig. 1.7. (**a**) Schematic of apparatus used for in situ measurement of carbon nanotube growth kinetics. A CW-HeNe laser beam is reflected from a vertically-standing substrate through the end window of a tube furnace. A remote microscope and video camera may be used from the opposite window to record growth to millimeters lengths. **(b)** Schematic of chemical vapor deposition (CVD) growth of vertically-aligned nanotube arrays (VANTAs). A thin film catalyst is deposited (usually 10 nm of Al as a buffer layer on Si, then ∼1 nm of Fe as catalyst, and sometimes ∼0.2 nm of Mo as a mixed catalyst). During heating in a tube furnace to 550–950 ° C in Ar/H_2 mixtures, the catalyst film roughens into nanoparticles. A mixture of hydrogen, argon and acetylene is then introduced (or another hydrocarbon such as methane, ethylene, etc.) and nanotubes nucleate and grow from the metal catalyst nanoparticles to form dense, self-aligned arrays. **(c)** SEM micrograph of a cleaved VANTA. The Si wafer is at the bottom, and the top of the array indicates the porous nature of the block of continuous nanotubes. Most VANTAs are <10 vol.% dense. **(d)** As the nanotubes begin to grow, the HeNe laser beam is reflected from both the metallized Si substrate and the top of the growing nanotube array, resulting in Fabry-Perot interference fringes measured at the detector (in addition to signal attenuation due to absorption). Each fringe corresponds to ∼300 nm of array height. The growth rate of the nanotubes can be directly measured in situ,and the length of the nanotube arrays can be controlled. After [23, 24]

to understand how the number of walls of a nanotube grown from a catalyst nanoparticle depends on the feedstock supply. The model predicts that for a particular catalyst the fastest growing nanotube is a SWNT at a given temperature and feedstock supply; however, with an oversupply of feedstock more nanotube walls are formed [30]. Typically, the number of walls found in continuously-grown VANTAs changes with time, as revealed by Raman spectroscopy in Fig. 1.8.

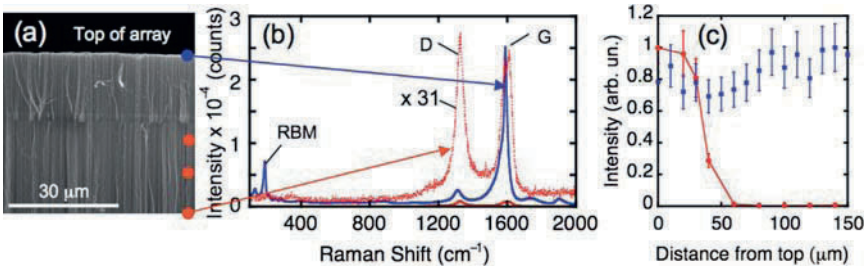

Fig. 1.8. (**a**) SEM image of the top of a VANTA array grown with different partial pressures of acetylene at 760 Torr 750° C in 2,500 sccm Ar/H_2 gas mixture. Since the nanotubes grow from catalyst anchored at the substrate, the top of the array (grown with 1 sccm C_2H_2) reflects nanotubes which grew first, and display a high SWNT fraction displaying (**b**) Raman spectra ($\lambda_{ex} = 633$ nm) with pronounced RBM modes and a high G/D Raman band ratio (*blue curve*). The number of walls in the array can be adjusted, in accordance with the growth model, by an oversupply in feedstock. Thus, the bottom part of the array (grown with 10 sccm C_2H_2) displays a lack of SWNTs and a Raman spectrum reflecting MWNTs (*red curves*, actual intensity and scaled by a factor of 31). (**c**) Raman profiling of the array (laser polarization parallel to the nanotube alignment) shows a dropoff in RBM intensity (*red circles and line*) following the change to 10 sccm feedstock supply after 15 μ of initial growth. An array grown at 1 sccm constant supply (*blue square points*) is shown for comparison [24]

Lasers, therefore, permit in situ remote characterization of nanotube growth kinetics via time-resolved reflectivity. Moreover, through Raman spectroscopy, the presence and diameter of SWNTs can be assessed through the presence of the radial breathing modes (RBMs) in micro-Raman profiling of nanotubes grown under different conditions (Fig. 1.8b). Similarly, the number of defects in the nanotubes can be assessed by a comparison of the G:D Raman band ratio intensity (Fig. 1.8c).

However, laser irradiation can also be used to alter the activity of the metal catalysts that are used for nanotube growth. Through KrF-laser processing of multilayer metal catalyst films prior to CVD, remarkable changes in subsequent VANTA growth rates, terminal heights, nanotube diameters, and wall numbers were observed [31]. Depending upon the fluence, growth was either stunted or enhanced; however, in the case of Fig. 1.9a the laser-processed regions resulted in over three times the growth rate and terminal length of the unprocessed regions, resulting in 1.4 cm-tall nanotube pillars. HRTEM analysis of the nanotubes in the tall pillars and shorter mats revealed a much narrower distribution of nanotube diameters and wall numbers in the laser-processed regions, corresponding to slimmer, faster-growing nanotubes. Despite their narrow diameter, the laser-processed regions were more densely packed; and weight measurements showed that on a *per unit substrate area* basis, the processed regions were *far* more catalytically active

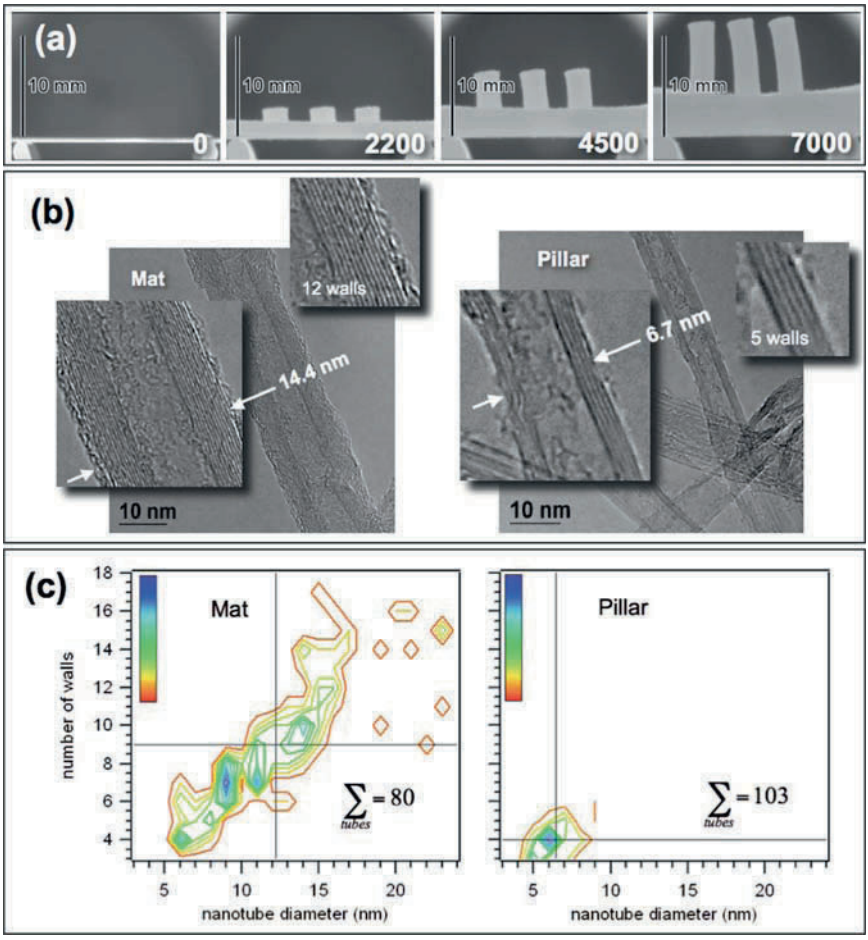

Fig. 1.9. (a) Time lapse images of VANTA growth on unprocessed and laser-irradiated Fe(1 nm)/Mo(0.2 nm) films on 10 nm Al-coated Si wafers, at the indicated time in seconds. **(b)**HRTEM images reveal that the taller pillars of nanotubes in the laser processed areas have ewer walls and are narrower in diameter than those in the mat (unirradiated area). **(c)** Distributions of nanotube wall number vs. nanotube diameter shows that the laser processed areas in the pillars have greatly reduced diameter distributions and smaller diameters. (Reproduced with permission from [31])

than the unprocessed area. Thus, laser processing appears highly promising to influence and control the catalytic activity of metal alloy films that are used for CVD.

Lasers can also be used to provide unique growth conditions for CVD. Recently, we utilized infrared laser pulses to provide well-defined growth periods for carbon nanotubes on Si wafers and TEM grids. As shown in Fig. 1.10,

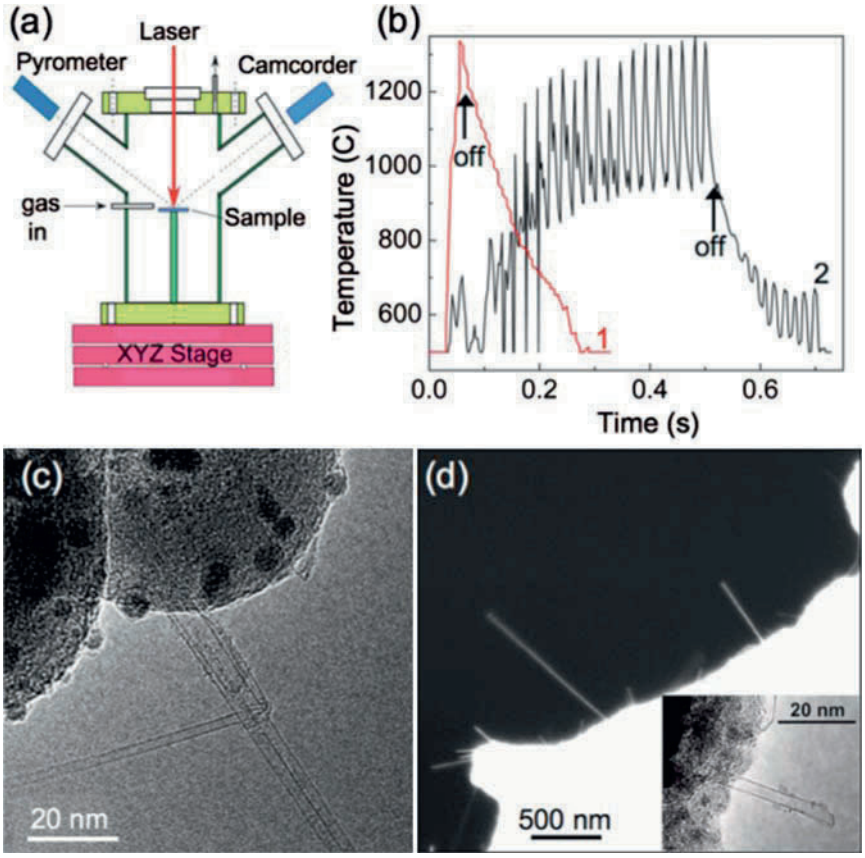

Fig. 1.10. (a) Schematic of PLA-CVD vacuum chamber. **(b)** Time-dependent temperature profile of a 1 cm^2 Si/SiO_2 wafer by a single 50 ms laser pulse (1), and a Mo TEM grid from 25 pulses of 5 ms width (2). *Arrows* show the time when laser irradiation is terminated. **(c)** TEM image of CNTs grown on a Mo grid coated with 1 nm Fe/Al_2O_3 by 1,500 laser pulses. **(d)** SEM of nanotubes grown using 20 pulses on an identically prepared grid as **(c)**. *Inset* shows a TEM image of the end of a nanotube free of catalyst particle [32]

laser heating of the substrates within a CVD chamber was monitored in situ by fast, optical pyrometry. The study found that exclusively SWNTs form by rapid laser heating, and at the highest recorded rates of $100\,\mu m\,sec^{-1}$ [32]. Interestingly, growth was found *not* to occur incrementally on successive laser pulses; that is, once the catalyst particle was cycled it was catalytically inactive. Nevertheless, on successive laser pulses new catalyst particles may nucleate and grow a nanotube. This feature was used to demonstrate the direct writing of SWNT field-effect transistors on prepatterned electrodes decorated with a catalyst [32].

1.7 Summary

In summary, a variety of laser interactions for nanomaterial synthesis have been described. Laser vaporization is a powerful exploratory tool in nanomaterial synthesis, providing congruent and complete vaporization of solids to permit the clean self-assembly of nanomaterials in gases, without interactions with substrates. Fullerenes, photoluminescent silicon quantum dots, and SWNHs are all examples of novel nanomaterials discovered by laser vaporization in different fluence ranges and background gas pressures.

Lasers are also used in the catalyst-assisted growth of nanomaterials, such as carbon nanotubes. Here, carbon nanotube growth by both laser vaporization and CVD were described. In both cases, laser interactions are used to remotely characterize the size, composition, and electronic structure of intermediate species and track their dynamics, as well as remotely provide some of the first-growth kinetics information of the nanotubes as they grow. During laser vaporization, laser-induced fluorescence and Rayleigh scattering utilizing time-delayed probe laser pulses were used to understand the timescales for growth. During CVD, time-resolved laser reflectivity from the growing nanotube arrays provides both length and density information of the arrays, and in situ Raman spectroscopy of SWNTs can be used to understand diameters and defects.

Lasers are emerging as instruments to modify and control growth, for example in the described laser processing of catalysts used for CVD to alter their activity, and also in the pulsed heating of metal catalysts to nucleate and grow discrete SWNTs in precise locations. A great variety of other effects remain to be described and explored; however, it is certain that lasers – with their remote delivery of energy – will be used to alter the synthesis conditions and characterize the effects for the growth of novel nanomaterials of the future.

Acknowledgments

The authors gratefully acknowledge the U.S. Dept. of Energy, Basic Energy Sciences Division of Materials Sciences and Engineering, for support of the synthesis science and the Scientific User Facilities Division for the development and support of the advanced characterization tools utilized in this work.

References

1. T.G. Dietz, M.A. Duncan, D.E. Powers, R.E. Smalley, J. Chem. Phys. **74**, 6511 (1981)
2. H.W. Kroto, J.R. Heath, S.C. O'Brien, R.F. Curl, R.E. Smalley, Nature **318**, 162 (1985)
3. A. Inam, X.D. Wu, T. Venkatesan, S.B. Ogale, C.C. Chang, D. Dijkkamp, Appl. Phys. Lett. **51**, 619 (1987)

4. D.B. Geohegan, Chap.4 in *Pulsed Laser Deposition of Thin Films*, ed. by D.B. Chrisey, G.K. Hubler (Wiley, New York, 1994)
5. A. Thess, R. Lee, P. Nikolaev, H. Dai, P. Petit, J. Robert, C. Xu, Y.H. Lee, S.G. Kim, A.G. Rinzler, D.T. Colbert, G.E. Scuseria, D. Tomanek, J.E. Fischer, R.E. Smalley, Science **273**, 483 (1996)
6. A.M. Morales, C.M. Lieber, Science **279**, 208 (1998)
7. X. Duan, C.M. Lieber, Adv. Mater. **12**, 298 (2000)
8. D.H. Lowndes, D.B. Geohegan, A.A. Puretzky, D.P. Norton, C.M. Rouleau, Science **273**, 898 (1996)
9. A.A. Puretzky, D.B. Geohegan, G.E. Jellison, M.M. McGibbon, Appl. Surf. Sci. **96–98**, 859 (1996)
10. A.A. Puretzky, D.B. Geohegan, X. Fan, S.J. Pennycook, Appl. Phys. Lett. **76**, 182 (2000)
11. R.F. Wood, K.R. Chen, J.N. Leboeuf, A.A. Puretzky, D.B. Geohegan, Phys. Rev. Lett. **79**, 1571 (1997)
12. R.F. Wood, J.N. Leboeuf, D.B. Geohegan, A.A. Puretzky, K.R. Chen, Phys. Rev. B **58**, 1533 (1998)
13. D.B. Geohegan, A.A. Puretzky, D.J. Rader, Appl. Phys. Lett. **74**, 3788 (1999)
14. H. Shinohara, Rep. Prog. Phys. **63**, 843 (2000)
15. C.N.R. Rao, G.U. Kulkarni, P.J. Thomas, Chap. 2 in *Springer Series in Materials Science 95*, ed. by C.N.R. Rao, G.U. Kulkarni, P.J. Thomas (Springer, Berlin, 2007)
16. Y.B. Zel'dowich, Y.P. Raizer, *Physics of Shock Waves and High-Temperature Hydrodynamic Phenomena* (Academic, New York, 1966)
17. D.B. Geohegan, A.A. Puretzky, G. Duscher, S.J. Pennycook, Appl. Phys. Lett. **72**, 2987 (1998); Appl. Phys. Lett. **73**, 438 (1998)
18. R.E. Smalley, Acc. Chem. Res. **25**, 98 (1992)
19. D.B. Geohegan, A.A. Puretzky, R.L. Hettich, X.-Y. Zheng, R.E. Haufler, R.N. Compton, Trans. Mat. Res. Soc. Jpn. **17**, 349 (1994)
20. S. Iijima, M. Yudasaka, R. Yamada, S. Bandow, K. Suenaga, F. Kokai, K. Takahashi, Chem. Phys. Lett. **309**, 165 (1999)
21. P.J.F. Harris, S.C. Tsang, J.B. Claridge, S.C. Sang, J.B. Claridge, M.L. Green, J. Chem. Soc. Faraday Trans. **90**, 2799 (1994)
22. D. Kasuya, M. Yudasaka, K. Takahashi, F. Kokai, S. Iijima, J. Phys. Chem. B **106**, 4947 (2002)
23. A.A. Puretzky, D.J. Styers-Barnett, C.M. Rouleau, H. Hu, B. Zhao, I.N. Ivanov, D.B. Geohegan, Appl. Phys. A. **93**(4), 849–855 (2008)
24. D. B. Geohegan, A.A. Puretzky, D. Styers-Barnett, H. Hu, B. Zhao, H. Cui, C.M. Rouleau, G. Eres, J.J. Jackson, R.F. Wood, S. Pannala, J.C. Wells, Phys. Stat. Sol. B **244**, 3944 (2007)
25. A. Thess, R. Lee, P. Nikolaev, H. Dai, P. Petit, J. Robert, C. Xu, Y.H. Lee, S.G. Kim, A.G. Rinzler, D.T. Colbert, G.E. Scuseria, D. Tomanek, J.E. Fischer, R.E. Smalley, Science **273**(5274), 483 (1996)
26. A.A. Puretzky, D.B. Geohegan, X. Fan, S.J. Pennycook, Appl. Phys. A **70**, 153 (2000)
27. A.A. Puretzky, H. Schittenhelm, X. Fan, M.J. Lance, L.F. Allard, D.B. Geohegan, Phys. Rev. B **65**, 245425/1 (2002)
28. D.B. Geohegan, A.A. Puretzky, I.N. Ivanov, S. Jesse, G. Eres, J.Y. Howe, Appl. Phys. Lett. **83**, 1851 (2003)

29. A.A. Puretzky, D.B. Geohegan, S. Jesse, I.N. Ivanov, G. Eres, Appl. Phys. A **81**, 223 (2005)
30. R.F. Wood, S. Pannala, J.C. Wells, A.A. Puretzky, D.B. Geohegan, Phys. Rev. B **75**, 235446 (2007)
31. C.M. Rouleau, G. Eres, H. Cui, H.M. Christen, A.A. Puretzky, D.B. Geohegan, Appl. Phys. A **93**(4), 1005–1009 (2008)
32. Z. Liu, D.J. Styers-Barnett, A.A. Puretzky, C.M. Rouleau, D. Yuan, I.N. Ivanov, K. Xiao, J. Liu, D.B. Geohegan, Appl. Phys. A **93**, 987 (2008)

2

Basic Physics of Femtosecond Laser Ablation

Juergen Reif

Summary. Laser ablation being the basic process for many prominent applications of lasers in present day high technology, medicine, and other fields, its basic physics is reviewed in this chapter. In order to distinguish the fundamental, laser–material interaction from any secondary effects, we concentrate on ultrashort laser pulses (≈100 fs duration) at comparably low intensities, below the commonly indicated threshold for massive material removal. It is shown that – for these conditions – the principal light/matter coupling occurs via multiphoton excitation of electrons into the conduction band or the vacuum. The resulting perturbation of the target lattice results in the emission of positive particles, from atomic ions to larger clusters of more than ten atoms. With the increasing number of incident pulses, the light/material coupling is facilitated by the accumulation of transient crystal defects resulting from particle removal. On the other hand, the lattice destabilization, upon excitation and ablation, relaxes via self-organized formation of regular nanostructures at the irradiated area. The strong influence of laser polarization on the structural order is still not at all understood.

2.1 Introduction

Already in the early days of lasers, it had been observed that the concentrated light energy could affect the irradiated material considerably: Damage to optical components occurred because of evaporation and removal of material from the component surface. In fact, that was the first manifestation of laser ablation, i.e. the removal of material from a target upon laser impact. Rapidly, this effect became exploited in a more controlled way to process materials, e.g. in tool-free cutting and drilling, which are standard technologies in the car industry and related fields today.

Most of the early research and applications were performed using CO_2 lasers, and understood in terms of the classical thermodynamic processes, the laser being considered merely as a very concentrated heat source. About three decades ago, however, based on the observation of UV-laser ablation from organic polymers [1], it was suggested that the ablation process might

be more complicated than had been assumed until then, involving not only rapid melting and evaporation but also electronic transitions. In the following years, the ablation phenomenon began to attract increasing interest, from the point of view of its fundamental study as well as its applications[2].

Today, laser ablation is used in a wide range of high technologies other than cutting and drilling, such as, for instance, surface processing, thin film deposition by PLD, or laser cleaning, from silicon wafers to artworks. In medicine also, many applications are based on laser ablation, e.g. in ophthalmology (amongst others, laser correction of ametropia – LASIK), dermatology (tattoo removal), surgery, etc. However, undesirable effects like the destruction of laser-irradiated biological tissue or laser damage to optical components also result from laser ablation.

This chapter is devoted to the study of the fundamental aspects of laser ablation in order to gain a better understanding of the physics underlying the phenomenon. In order to distinguish the basic processes from any secondary effects, such as laser interaction with ablation products and the like, we concentrate on the interaction of ultrashort (i.e. duration of $\approx$100 fs) laser pulses with solid targets. To further reduce secondary effects, the incident fluence is so low that single pulses do not result in significant, target surface modification. Usually, only after several 10,000 pulses, significant ablation craters are observed. Our sample materials will be mainly dielectrics (BaF_2, CaF_2, Al_2O_3), and silicon. We first review some basic features of the energy input, the laser–material coupling. Then we consider the follow-up processes, transiently modifying the material. Finally, we report on self-organized, nanostructure formation at the target surface as a consequence of material relaxation after ablation.

2.2 Energy Input

In principle, all decomposition or material removal from a solid target is the consequence of an energy input into the target, resulting in overcoming the solid's binding energy. In a classical process, which is slow enough to proceed in thermodynamic equilibrium, this means that the energy input ΔE is fully transferred into an increase of internal energy ΔU and thus, to an increase in temperature ΔT:

$$\Delta E = \Delta U = cm\Delta T \tag{2.1}$$

(with heat capacity c and mass m of the heated target material).

As shown in Fig. 2.1, this internal energy increase results in a classical phase transition and, occasionally, in a dissolution of the heated volume. On a microscopic scale, the temperature increase corresponds to an increase of atomic kinetic energy. In contrast to energy input by classical heating, via a global phonon bath, or by ion impact, addressing the core motion directly via a momentum transfer, energy input from laser pulses is inherently different:

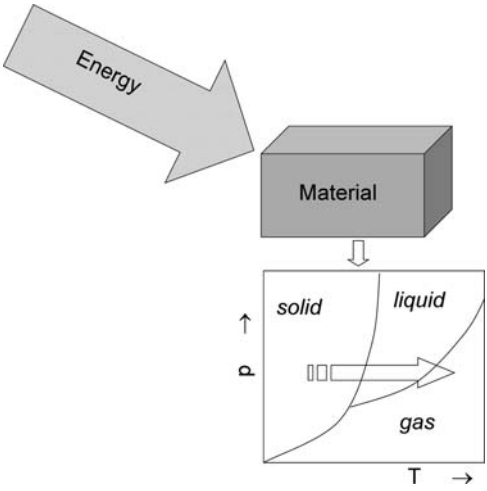

Fig. 2.1. Schematic representation of energy input into a solid material

Table 2.1. Process chart for laser ablation

Time scale	Material response	Observation
Femtoseconds	Electronic excitation	Electron emission
Picoseconds	Energy dissipation/ core motion	
	Bond breaking	Atom/ion emission
Nanoseconds		(Plasma) plume
	Surface relaxation/ reorganization	

the incident light "speaks" only to the electrons of the system, and all core motion is only a *secondary* process.[1] This allows establishing, conceptually, a history of processes starting from light absorption, leading to particle removal and, finally, to target relaxation, as is given in Table 2.1.

From these time scales, the choice of ultrashort laser pulses with duration below 150 fs for the study of fundamentals becomes justified: then, the laser light interacts only with an almost passive target. All significant target modification (e.g. transient changes in band-structure, removal of particles) occurs only *after* the laser pulse and, thus, should not affect the absorption properties. More important, the laser does not interact with ablated material. (For longer pulses, significant amounts of laser energy may be absorbed in the ablated plasma plume. This hot plasma might then, in turn, sputter the target surface.)

[1] Even a direct coupling to a vibration is, in fact, promoted via the *electronic* system, related to the cores only by electron–phonon coupling.